NeuroImage: Clinical 35 (2022) 103086

Contents lists available at ScienceDirect

NeuroImage: Clinical

journal homepage: www.elsevier.com/locate/ynicl

Thalamic-insomnia phenotype in E200K Creutzfeldt–Jakob disease: A PET/MRI study

Hong Ye [1], Min Chu [1], Zhongyun Chen, Kexin Xie, Li Liu, Haitian Nan, Yue Cui, Jing Zhang, Lin Wang, Junjie Li, Liyong Wu [*]

Department of Neurology, Xuanwu Hospital, Capital Medical University, Beijing, China

ARTICLE INFO

Keywords:
Creutzfeldt–Jakob disease
Thalamus
Insomnia
PRNP gene
E200K
PET/MRI

ABSTRACT

Background: Insomnia and thalamic involvement were frequently reported in patients with genetic Creutzfeldt-Jakob disease (gCJD) with E200K mutations, suggesting E200K might have discrepancy with typical sporadic CJD (sCJD). The study aimed to explore the clinical and neuroimage characteristics of genetic E200K CJD patients by comprehensive neuroimage analysis.

Methods: Six patients with gCJD carried E200K mutation on Prion Protein (PRNP) gene, 13 patients with sporadic CJD, and 22 age- and sex-matched normal controls were enrolled in the study. All participants completed a hybrid positron emission tomography/magnetic resonance imaging (PET/MRI) examination. Signal intensity on diffusion-weighted imaging (DWI) and metabolism on PET were visually rating analyzed, statistical parameter mapping analysis was performed on PET and 3D-T1 images. Clinical and imaging characteristics were compared between the E200K, sCJD, and control groups.

Results: There was no group difference in age or gender among the E200K, sCJD, and control groups. Insomnia was a primary complaint in patients with E200K gCJD (4/2 versus 1/12, $p = 0.007$). Hyperintensity on DWI and hypometabolism on PET of the thalamus were observed during visual rating analysis of images in patients with E200K gCJD. Gray matter atrophy (uncorrected $p < 0.001$) and hypometabolism (uncorrected $p < 0.001$) of the thalamus were more pronounced in patients with E200K gCJD.

Conclusion: The clinical and imaging characteristics of patients with gCJD with PRNP E200K mutations manifested as a thalamic-insomnia phenotype. PET is a sensitive approach to help identify the functional changes in the thalamus in prion disease.

1. Introduction

Creutzfeldt–Jakob disease (CJD) is a rare, fatal prion disease characterized by rapidly progressive dementia, gait disturbance, myoclonus, visual or cerebellar symptoms, pyramidal or extrapyramidal dysfunction, and akinetic mutism (Hermann et al., 2021). Creutzfeldt–Jakob disease mainly includes sporadic CJD (sCJD) and genetic CJD (gCJD) (Knight and Will, 2004). Most of the CJD diagnosis are sporadic, while approximately 10–15% of cases explained by genetic variants, including a point mutation or an insertion of octapeptide repeats in the prion protein (PRNP) gene (Chen and Dong, 2016). Mutation of PRNP E200K is frequently observed in gCJD, and there are approximately 1,200 patients with E200K gCJD worldwide, some of whom were reported to have symptoms and pathological changes inconsistent with a typical sCJD (Heinemann et al., 2007; Kovács et al., 2005).

Clinical and imaging differences between E200K gCJD and sCJD are not well understood. Some publications have reported insomnia and autonomic disturbance in patients with PRNP E200K mutations, which is not consistent with typical sCJD, and is more similar to fatal familial insomnia (FFI), another type of prion disease resulting from PRNP D178N mutations that impacts the thalamus (Chapman et al., 1996; Feketeova et al., 2019; George et al., 2017; Taratuto et al., 2002). Approximately 21% of the patients with E200K mutations had abnormally high thalamic signal on diffusion-weighted imaging (DWI), which indicated that the thalamus may be vulnerable in patients with gCJD with E200K mutations (Kovacs et al., 2011). Positron emission tomography (PET) is critical to early diagnosis of CJD due to high sensitivity (Qi et al., 2020). However, the role of thalamus hypometabolism in

* Corresponding author.
E-mail address: cmsddhr@sina.com (L. Wu).
[1] These authors contributed equally to this work.

https://doi.org/10.1016/j.nicl.2022.103086
Received 2 February 2022; Received in revised form 12 May 2022; Accepted 13 June 2022
Available online 18 June 2022

patients with E200K has not been extensively studied. In addition, no study has used quantitative analysis of 3D-T1 gray matter volume in patients with PRNP with E200K.

In this study, we consecutively enrolled 6 patients with E200K, 13 patients with sCJD, and 22 age- and sex-matched normal controls and used hybrid PET/MRI scans to investigate structural and metabolic changes in the brain. This study examined the clinical and neuroimaging characteristics of patients with E200K and identified whether the thalamus was more vulnerable in patients with E200K mutations than in patients with sCJD. Based on previous publications, we hypothesized that E200K mutations might cause thalamic impairment, which may be associated with sleep disturbance.

2. Methods

2.1. Ethics

This study was conducted in accordance with the Declaration of Helsinki. The clinical protocols were approved by the ethics committee and local institutional review board of Xuanwu Hospital, Capital Medical University, China. The study was conducted in accordance with relevant guidelines and regulations for use of human subjects in research. Written informed consent was obtained from all participants or their guardians before the start of the study.

2.2. Subjects

Six patients with E200K gCJD, 13 patients with sCJD, and 22 age- and sex-matched normal controls were enrolled in the study from July 1, 2017, to October 31, 2021 in the Department of Neurology at Xuanwu Hospital. All patients were clinically diagnosed as probable CJD cases (Hermann et al., 2021). All patients completed PRNP gene analysis, and patients with PRNP E200K mutations were included in the E200K gCJD group. Patients negative for PRNP mutations were placed in the sCJD group. Exclusion criteria included: 1) other causes of cognitive impairment, including small vessel disease, stroke, infection, autoimmune diseases, metabolic diseases, and other neurodegenerative diseases except for CJD; 2) inability to undergo PET/MRI examination, or an inability to comply with study instructions, including patients who had severe psychiatric symptoms or severe disease condition (CDR sum of box > 12 points); 3) history of traumatic brain injury; 4) history of psychosis (including schizophrenia and bipolar affective disease) or congenital cognitive deficits; or 5) any form of mutation in the PRNP gene except E200K. According to the exclusion criteria, we excluded 2 patients with schizophrenia and 1 patient with bipolar affective disease, 2 sCJD patients with severe psychiatric symptoms who could not cooperate to undergo PET/MRI examination, and 3 patients in severe disease condition with CDR sum of box > 12 points.

2.3. Electroencephalogram

All subjects underwent a 2 h electroencephalogram (EEG) using an 18-lead electroencephalographic transducer (Micromed, Italy). Electrodes were placed in accordance with the international standard 10–20 system. Conventional single, double, and sphenoid leads were traced. Periodic sharp wave complexes (PSWCs) were visually screened on the EEG.

2.4. PET/MRI acquisition parameters

All images were acquired on a hybrid 3.0 T TOF PET/MRI scanner (SIGNA PET/MR, GE Healthcare, WI, USA). PET and MRI data were acquired simultaneously using a vendor-supplied 19-channel head and neck union coil. Each subject was asked to fast for at least 6 h to reach serum glucose levels of lower than 9 mmol/L. Each patient received an intravenous injection of 3.7 MBq/kg ^{18}F-FDG. Subjects were asked to wait at least 30 min before FDG administration and during the brain uptake phase.

Sequences included a rapid scout, followed by DWI using a single-shot, echo-planar, spin-echo sequence acquired in the axial-oblique plane with parameters of TR 5000 ms, TE 85 ms, FOV of 24 cm, and imaging matrix of 128 × 128, with b-values of 0 s/mm2 (T2-weighted image) and 1000 s/mm2 along three orthogonal directions, and 3-mm contiguous sections resulting in 48 sections. The average DWI image was calculated as the mean of the individual signal intensities in each of the three orthogonal diffusion vector directions. An ADC map (in units of μm2/s) was constructed automatically from the average DWI image and the T2-weighted image (b = 0) using standard formulas.

A FLAIR sequence had parameters of TR 9000 ms, TE 120 ms, and TI 2200 ms, and a T2-weighted fast spin-echo (FSE) sequence had parameters of TR 4000 ms, TE 90 ms, and an echo-train length of 9. Both the FLAIR and FSE sequences were acquired in the axial-oblique plane and had an FOV of 24 cm, an imaging matrix of 256 × 256, 3-mm-thick sections with a 3-mm gap, and 24 sections that were positioned so that their centers coincided with every other DWI section. The parameters of the T1 data were as follows: repetition time (TR) = 6.9 ms, echo time (TE) = 2.98 ms, flip angle = 12∘, inversion time = 450 ms, matrix size = 256 × 256, field of view (FOV) = 256 × 256 mm^2, slice thickness = 1 mm, 192 sagittal slices with no gap, voxel size = 1 × 1 × 1 mm^3, and acquisition time = 4 min 48 s.

Static ^{18}F-FDG-PET data were acquired in list mode for 30 min and 89 slices were captured to encompass the entire brain, using the following parameters: matrix size: 192 × 192, FOV: 350 × 350 mm^2, and pixel size: 1.82 × 1.82 × 2.78 mm^3. Corrections were made for random coincidences, dead time, scatter, and photon attenuation. Attenuation correction was performed based on MR imaging of the brain (Atlas-based co-registration of 2-point Dixon). The default attenuation correction sequence was automatically determined and acquired as follows: LAVA-Flex (GE Healthcare) axial acquisition, TR: 4 ms, TE: 1.7 ms, slice thickness: 5.2 mm with a 2.6-mm overlap, 120 slices, pixel size: 1.95 × 2.93 mm, and acquisition time: 18 s. The images were reconstructed with a time-of-flight point spread function and the order subset expectation maximization (TOF-PSF-OSEM) algorithm (32 subsets 8 iterations and a 3-mm cut-off filter).

2.5. DWI hyperintensity/ PET hypometabolism visual assessment

The data for each subject were deidentified and randomized. The data were in a DICOM format and were analyzed by using DICOM viewing software. Two independent raters blinded to subject identity and diagnosis visually evaluated the DWI images, ADC maps and PET images. Firstly, we divided the whole brain into 26 cortical and 5 subcortical subdivisions (Eisenmenger et al., 2016; Vitali et al., 2011). Then we used a semiquantitative scoring system that drew a region of interest in normal-appearing white matter and compared the mean signal intensity (SI) in these brain regions visually thought to be normal (score 0, with the SI within 2SDs of the white matter SI), mild hyperintense (score 1, with the SI>2SDs above the white matter SI), and clear hyperintense (score 2, with the SI at least 2 times the white matter SI). To differentiate the artifactual cortical DWI hyperintensity from the true high SI, we also examined the ADC map to make sure the corresponding areas of hypo-intensity. As for FDG PET, using the same brain template, we calculated the mean and SD of SUVR in the normal control group and make a comparison between each CJD patients and control. We defined normal (score 0, the SUVR value of CJD patient is within 2SDs of the mean value for the normal control), mild hypometabolism (score 1, the SUVR values of CJD patient is 2SDs below the mean value for the normal control), and clear hypometabolism (score 2, the SUVR values of CJD patient is 3SDs below the mean value for the normal control).

Table 1
Demographic and clinical data from patients with E200K gCJD (n = 6), patients with sCJD (n = 13) and normal controls (n = 22).

	E200K (n = 6)	sCJD (n = 13)	NC (n = 22)	*p*
Age (years)	49.0 ± 7.1	55.0 ± 4.9	52.7 ± 7.3	0.193
Gender (male/female)	3/3	4/9	11/11	0.513
Survival time	14.7 ± 6.1	9.7 ± 6.9	/	0.140
Disease duration (month)	2.0 ± 0.9	1.5 ± 0.8	/	0.246
Clinical features				
Insomnia	4/2	1/12	/	0.007
RPD	2/4	10/3	/	0.067
Myoclonus	3/3	5/8	/	0.636
Visual sign	1/5	2/11	/	0.943
Cerebellar sign	5/1	8/5	/	0.342
Extrapyramidal features	4/2	3/10	/	0.067
Pyramidal features	4/2	4/9	/	0.141
Auxiliary examination				
MMSE	18.7 ± 9.3	16.5 ± 5.3	/	0.628
CDR sum of box	2.7 ± 1.0	5.1 ± 3.6	/	0.119
NPI-patient	12.0 ± 2.0	20.4 ± 16.24	/	0.411
NPI-caregiver	3.0 ± 1.7	7.0 ± 6.5	/	0.367
MRC-PDR	11.2 ± 4.5	0.9 ± 3.4	/	0.897
EEG PSWCs	2/4	6/7	/	0.577
1433 protein (P/N/NA)	1/2/3	6/7/0	/	0.687
129 polymorphisms				
MM/MV	6/0	12/1	/	0.485

Abbreviations: sCJD, sporadic CJD; NC, normal control; RPD, rapid progressive dementia; MMSE, Mini-mental State Examination; CDR, Clinical Dementia Rating; NPI, Neuropsychiatric inventory; MRC-PDR, the medical research counsel prion disease rating scale; EEG, electroencephalogram; PSWCs, periodic sharp wave complexes. P, positive; N, negative; NA, not available.

2.6. PET/MRI image preprocessing

Structural images were preprocessed using the computational anatomy toolbox 12 (CAT 12), which is based on statistical parametric mapping 12 (SPM12), and is used in MATLAB (MathWorks, Natick, Massachusetts). The DICOM files were converted to nifti format. Voxel-based morphometry (VBM) preprocessing was performed using the default settings of the CAT12 toolbox and the "East Asian Brains" ICBM template. T1-weighted 3D images were segmented into gray matter (GM), white matter (WM), and cerebrospinal fluid partitions. Subsequently, the GM and WM partitions of each subject in native space were high-dimensionally registered and normalized to the standard Montreal Neurological Institute (MNI) space using diffeomorphic anatomical registration through exponentiated lie algebra normalization. The images were then smoothed using an 8-mm full-width half-maximum Gaussian kernel.

PET images were preprocessed using SPM12, implemented in MATLAB (MathWorks, Natick, Massachusetts). After spatial normalization of the structural MR images to standard Montreal Neurological Institute (MNI) space using diffeomorphic anatomical registration through exponentiated lie algebra normalization, the transformation parameters determined by the T1-weighted image spatial normalization were applied to the co-registered PET images for PET spatial normalization. The images were then smoothed using an 8-mm full-width half-maximum isotropic Gaussian kernel. Finally, PET scan intensity was normalized using a whole cerebellum reference region to create standardized uptake value ratio (SUVR) images.

2.7. Statistical analysis

Statistical analysis of PET/MRI images was performed using SPM12, implemented in MATLAB (MathWorks, Natick, Massachusetts). The processed 3D-T1 MRI and ^{18}F-FDG PET data were used to perform voxel-wise whole-brain comparisons. Two tailed *t*-test was used to compare between gCJD with E200K Vs normal controls, sCJD Vs normal controls, and gCJD with E200K Vs sCJD, with age and sex as covariates. The threshold was then set to uncorrected $p < 0.001$. Statistical analyses of demographic data were carried out in SPSS 22.0 (IBM Corporation, Armonk, NY, USA). Continuous data are represented as means ± standard deviations. Dichotomous data are represented as absolute values. Group differences were evaluated using one-way ANOVA for continuous data, and chi-square test for categorical data. Statistical significance of demographic data was set at $p < 0.05$.

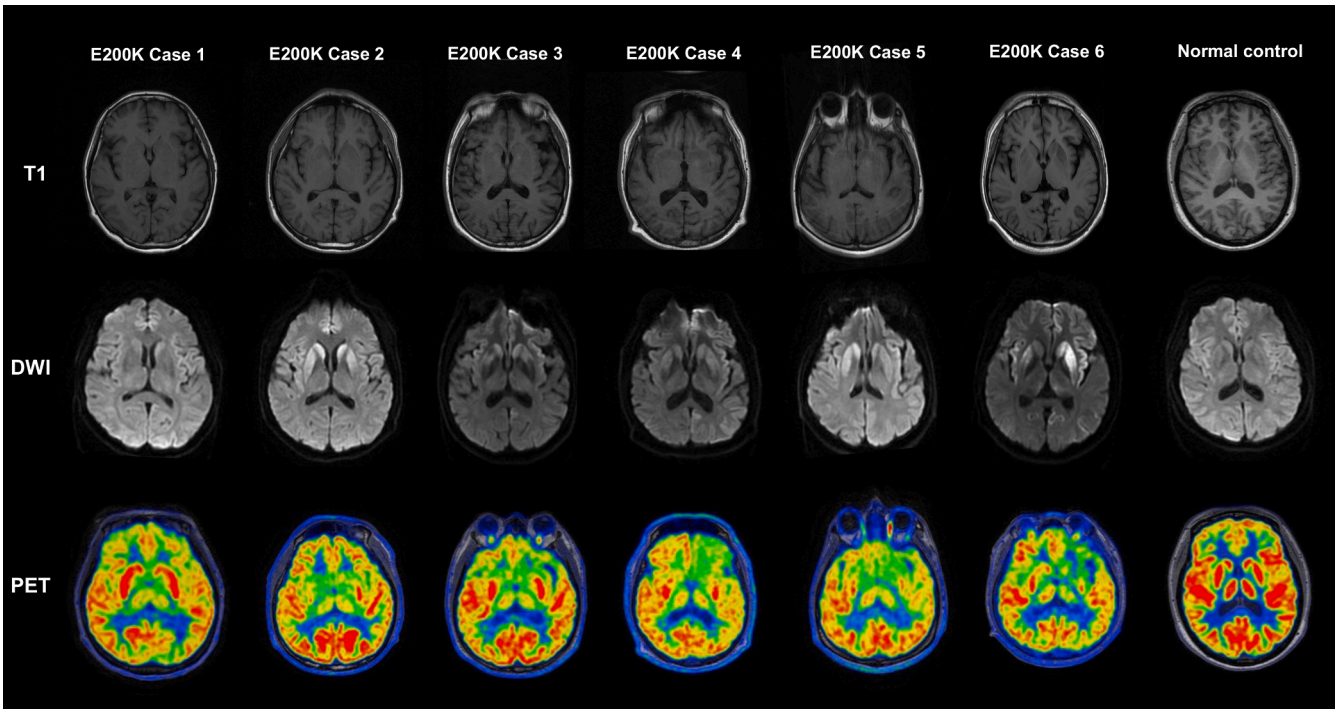

Fig. 1. T1, DWI and FDG-PET images of six patients with E200K gCJD and normal control.

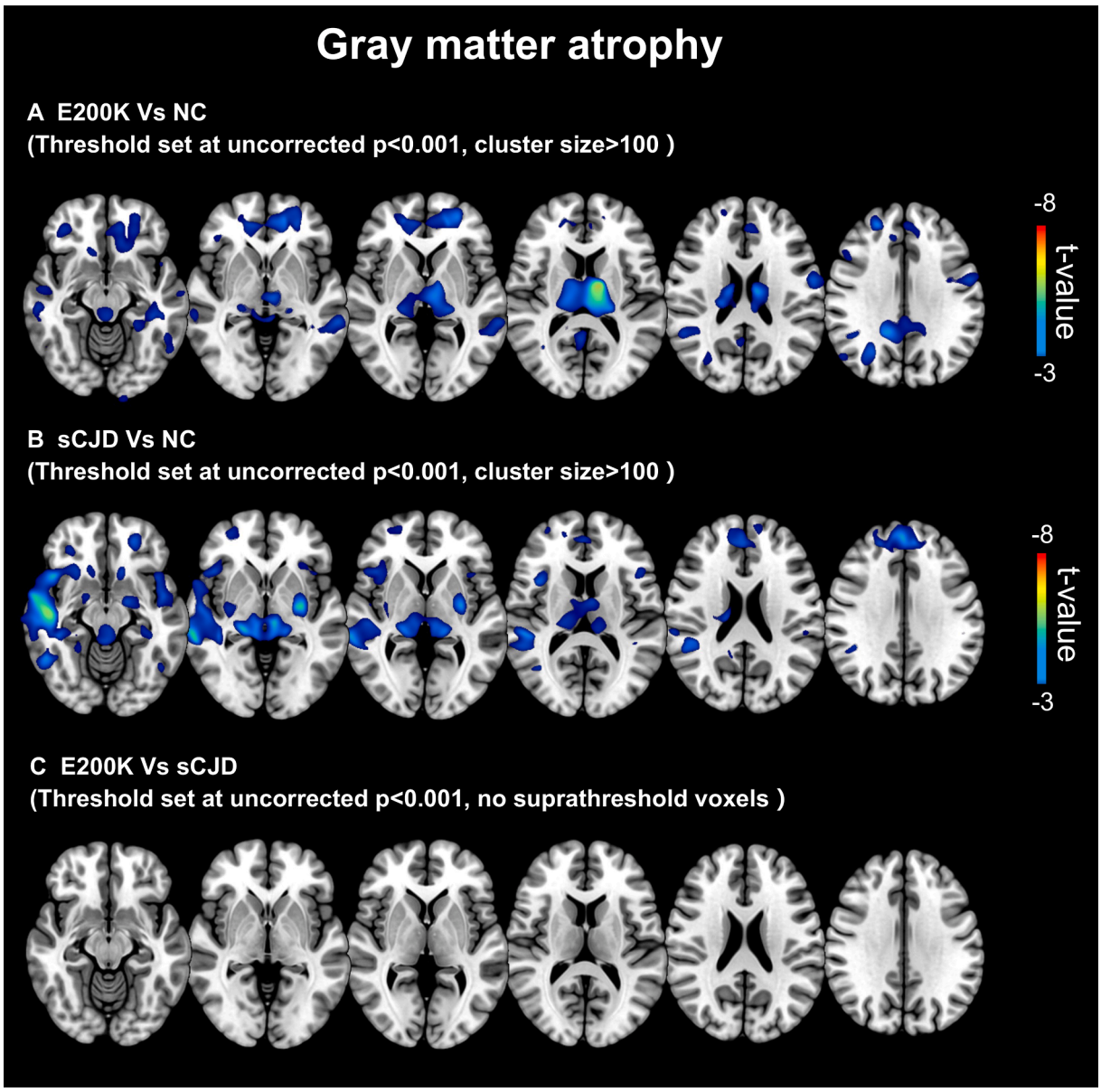

Fig. 2. Gray matter atrophy profiles. A) Regions of gray matter atrophy in patients with E200K gCJD compared with those in normal controls; B) Regions of gray matter atrophy in patients with sCJD compared with those in normal controls; C) Differences in gray matter atrophy between patients with E200K gCJD and sCJD. (All thresholds set at uncorrected $p < 0.001$, cluster size > 100).

3. Results

3.1. Participant demographics and raw image data

Detailed demographic data are summarized in Table 1. Six patients with E200K were enrolled, of which three were men and three were women. There were no group differences in age (49.0 ± 7.1, 55.0 ± 4.9, and 52.7 ± 7.3 for E200K, sCJD, and control, respectively; $p = 0.193$) and gender (M/F; 3/3, 4/9, and 11/11 for E200K, sCJD, and control, respectively; $p = 0.513$) between patients with E200K, sCJD and normal controls. Insomnia was a major complaint in patients with E200K (E200K Vs sCJD, insomnia/no insomnia, 4/2 versus 1/12, $p = 0.007$).

Raw image data for 3D-T1, DWI and PET are shown in Fig. 1. All patients with E200K had hypometabolism in the thalamus, two patients (Patient 2 and Patient 6) had high signal in the DWI sequence, and no patients observed thalamic atrophy visually.

3.2. Visual rating analysis

When comparing DWI images of E200K group with sCJD group (shown in Supplementary Fig. 1), the signal intensity of left anterolateral (0.67 ± 0.52 Vs 0.08 ± 0.28, $p = 0.037$) and posteromedial thalamus (0.67 ± 0.52 Vs 0.15 ± 0.38, $p = 0.025$) was higher in E200K group than sCJD group. When compared PET images of E200K group and sCJD group (shown in Supplementary Fig. 2), the hypometabolism brain regions were in left lingual (1.50 ± 0.55 Vs 0.62 ± 0.77, $p = 0.036$), left fusiform occipital (1.67 ± 0.52 Vs 0.85 ± 0.80, $p = 0.022$), left putamen (1.33 ± 1.03 Vs 0.46 ± 0.66, $p = 0.039$), left anterolateral thalamus (1.83 ± 0.41 Vs 0.31 ± 0.63, $p < 0.001$) and posteromedial thalamus (1.67 ± 0.52 Vs 0.23 ± 0.60, $p < 0.001$), right anterolateral thalamus (1.83 ± 0.41 Vs 0.31 ± 0.63, $p < 0.001$) and posteromedial thalamus (1.5 ± 0.55 Vs 0.31 ± 0.63, $p = 0.001$).

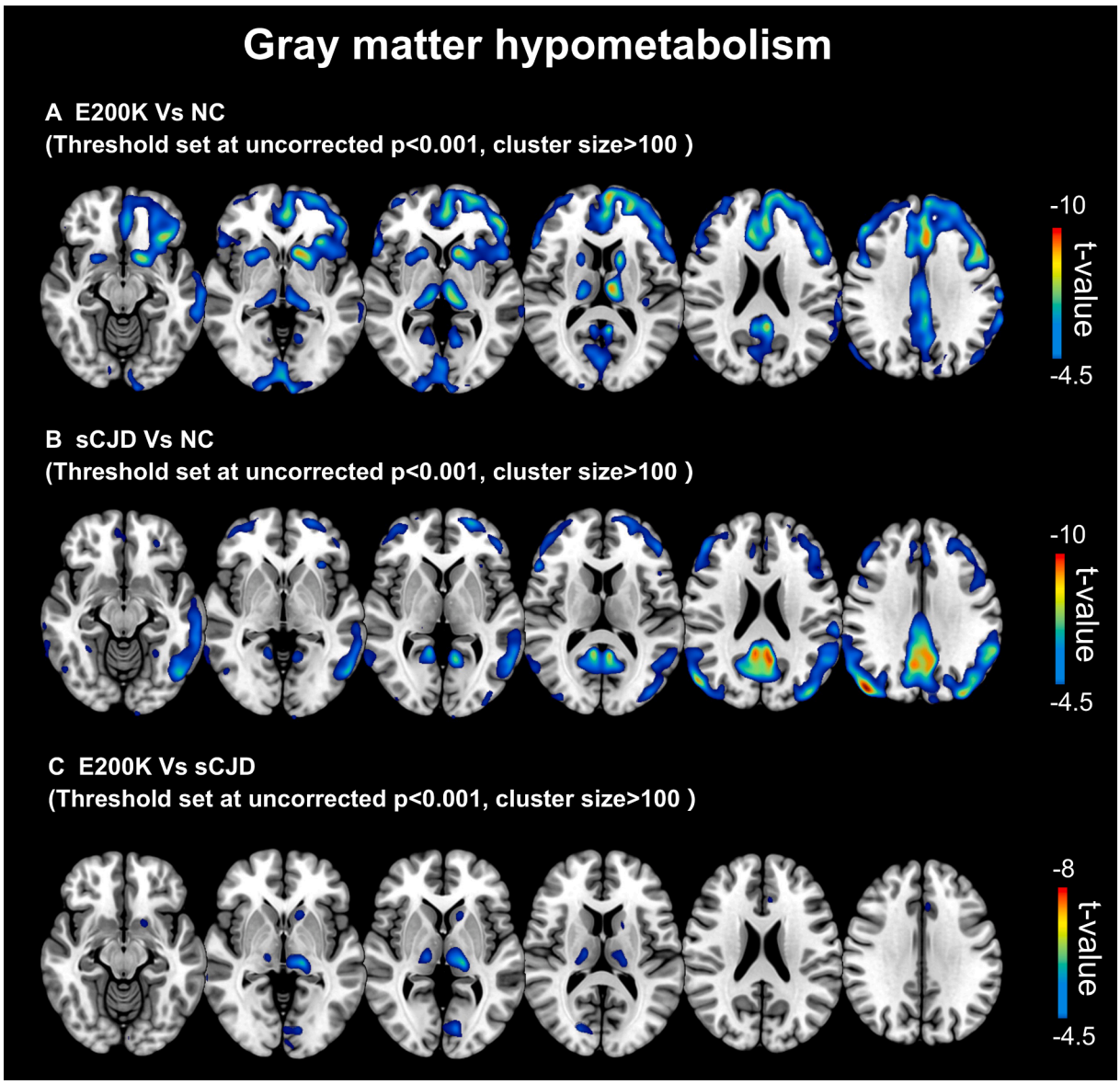

Fig. 3. Gray matter hypometabolism profiles. A) Regions of gray matter hypometabolism in patients with E200K patients compared with those in normal controls; B) Regions of gray matter hypometabolism in patients with sCJD compared with those in normal controls.; (C) Differences in gray matter hypometabolism between patients with E200K and sCJD (All threshold set at uncorrected $p < 0.001$, cluster size > 100).

3.3. GM atrophy and hypometabolism profiles

Statistical parametric mapping (SPM) of gray matter atrophy and hypometabolism patterns are shown in Figure-2 and Figure-3. In Fig. 2-A, when comparing E200K group with normal controls, GM volume was decreased the bilateral thalamus, right middle temporal cortex, and right middle cingulate (Uncorrected $p < 0.001$). When comparing sCJD group with normal controls (Fig. 2-B), GM volume decreased in the right middle temporal cortex, bilateral superior temporal pole, right inferior temporal cortex, left middle temporal pole, left superior medial frontal cortex, right inferior orbital frontal cortex, right superior frontal cortex, left superior orbital frontal cortex, left middle orbital frontal cortex, bilateral thalamus, and left putamen (Uncorrected $p < 0.001$). No voxels survived at uncorrected $p < 0.001$ when comparing GM volumes between the E200K group and sCJD group (Fig. 2-C).

As shown in Fig. 3-A, when comparing the E200K group with normal controls, GM hypometabolism regions were observed in the bilateral middle frontal cortex, left superior frontal cortex, bilateral superior temporal cortex, left cingulate, left superior parietal cortex, left middle occipital cortex, right superior occipital cortex, left putamen and bilateral thalamus (Uncorrected $p < 0.001$). When comparing sCJD group with normal controls (Fig. 3-B), GM hypometabolism regions were observed in the left precuneus, left superior frontal cortex, bilateral middle frontal cortex, bilateral middle temporal cortex, and left superior parietal cortex, right middle occipital cortex (Uncorrected $p < 0.001$). When comparing the E200K group with the sCJD group (Fig. 3-C), GM metabolism was observed lower in the bilateral thalamus, left lingual cortex, left putamen, and left anterior cingulate (Uncorrected $p < 0.001$). Spatial coordinates and peak values of brain areas of GM atrophy and hypometabolism are shown in Table 2.

4. Discussion

In this study, we confirmed thalamic involvement in insomnia in six consecutive patients with E200K gCJD based on quantitative analysis of hybrid PET/MRI images. Our study provided evidence that E200K gCJD had different phenotype than sCJD based on clinical and neuroimaging profiles, and that the thalamus, which can be involved in insomnia, was

Table 2
Spatial coordinates and peak values of brain areas showing significant differences in gray matter volume and metabolism among patients with E200K gCJD, patients with sCJD, and normal controls (All threshold set at uncorrected $p < 0.001$, cluster size > 100).

	Side	MNI coordinate	Cluster size	T value
Atrophy E200K Vs NC				
Thalamus	L	−12 −7.5 12	1644	−5.68
Thalamus	R	14.5 −12 16	318	−4.56
Middle Temporal Pole	R	33 12 −38	391	−5.18
Middle Cingulum	R	13.5 −48 33	144	−4.89
Atrophy sCJD Vs NC				
Middle Temporal	R	57.5 −12 −21	2076	−6.02
Superior Temporal pole	R	50 14 −18	1540	−6.02
Inferior Temporal	R	52.5 −54 −13.5	177	−4.45
Superior Temporal Pole	L	−48 1.5 −16.5	650	−5.04
Middle Temporal Pole	L	−42 10 −32	242	−4.48
Superior Medial Frontal	L	1.5 49.5 31.5	852	−4.54
Inferior Orbital Frontal	R	24 20 −20	222	−4.50
Superior Frontal	R	24 44 40	210	−4.52
Superior Orbital Frontal	L	−12 21 −18	125	−4.90
Middle Orbital Frontal	L	−33 43 −12	110	−4.77
Thalamus	L	−7.5 −22.5 4.5	281	−5.14
Thalamus	R	19.5 −28.5 3	342	−4.95
Putamen	L	−29 −9 −2	518	−5.11
Atrophy E200K Vs sCJD (No suprathreshold voxels)				
Hypometabolism E200KVs NC				
Middle Frontal	L	−35 17 34	4311	−8.24
Superior Frontal	L	−20 59 18	3208	−8.82
Middle Frontal	R	28 26 34	3779	−8.95
Superior Temporal	L	−47 −23 5.5	1088	−7.56
Superior Temporal	R	55 −24 6	128	−4.50
Cingulate	L	−6 −52 18	4290	−8.95
Superior parietal	R	28 −54 55	1387	−8.04
Middle Occipital	L	−51 −76 2	906	−8.24
Superior Occipital	R	22 −88 12	361	−7.24
Putamen	L	−20 2 11	971	−9.06
Thalamus	L	−6 −18 8	870	−9.90
Thalamus	R	12 −22 6	749	−7.48
Hypometabolism sCJD Vs NC				
Precuneus	L	−8 −60 43	6404	−9.92
Superior Frontal	L	−22 62 6	6072	−9.31
Middle Frontal	L	−26 22 42	3401	−6.52
Middle Frontal	R	48 42 20	3556	−6.57
Middle temporal	R	52 −26 −8	2532	−6.76
Middle temporal	L	−57 −29 −8	5661	−6.76
Superior Parietal	L	−17 −66 42	1486	−8.54
Middle Occipital	R	38 −69 32	1961	−9.92
Hypometabolism E200K Vs sCJD				
Thalamus	L	−16 −24 0	553	−6.95
Thalamus	R	14 −18 6	344	−5.61
Lingual	L	−12 −82 2	390	−5.67
Putamen	L	−18 14 0	278	−4.73
Anterior Cingulum	L	−6 32 18	192	−4.61

more frequently impaired in patients with E200K gCJD than in patients with sCJD.

No group analysis studies using hybrid PET/MRI imaging of gCJD had been performed previously, and previous publications are just visual analysis reports of individual E200K gCJD cases. Therefore, our small cohort studies can better represent the structural and metabolic characteristics of patients with E200K gCJD. Furthermore, no previous studies have compared E200K gCJD and sCJD. Our study was the first to use quantitative analysis to show differences in clinical and functional characteristics between E200K gCJD and sCJD. In addition, our quantitative results are reliable because it was mostly consistent with the results of visual analyses using PET or MRI in previous case reports.

Our study provided evidence that E200K gCJD may mimic the thalamic-insomnia phenotype that is characteristic of FFI. In our study, thalamic impairment was observed in DWI analyses, GM volume, and GM metabolism in patients with E200K gCJD. This finding is consistent with those of previous studies showing thalamic involvement using SPECT (Konno et al., 2008), PET (George et al., 2017), and pathological evidence (two case studies) (Chapman et al., 1996; Taratuto et al., 2002). In addition, an ADC study of E200K carriers showed early involvement of thalamo-striatal neuronal circuits during the preclinical to clinical transition phase, which supported thalamic vulnerability in E200K gCJD (Cohen et al., 2015a). Insomnia was a common symptom in our E200K group and is not a classical symptom of sCJD. This finding was in line with the results of studies using polysomnography that reported sleep disturbances in patients with E200K gCJD patients, including sleep fragmentation, loss of sleep spindles, and decreased rapid eye movement (REM) sleep time (Cohen et al., 2015b; Givaty et al., 2016) The thalamus plays a critical role in sleep-related physiological phenomena, and thalamic dysfunction might contribute to the neurobiological mechanisms underlying insomnia. Previous studies showed that thalamic reticular nucleus neurons were associated with generation of sleep spindles and regulated sleep and awake states (Marini et al., 2000; Saper et al., 2005; Steriade et al., 1985). These insights support the potential association of thalamic impairment and insomnia in patients with E200K.

We observed a trend toward a decrease in GM volume of the thalamus and cortex in E200K gCJD. However, functional changes are more pronounced and can be more easily detected using PET. In our study, all patients with E200K gCJD had thalamic hypometabolism on PET, but only two were noted high DWI signal, which indicated that PET may provide additional information beyond DWI when visually inspection. Nerve cell loss, spongiform degeneration, and astrocyte gliosis can all contribute to DWI hyperintensity (Chung et al., 1999; Manners et al., 2009), but definite mechanisms have not been clarified, and as the course progresses, the signals of the DWI and ADC may convert, which may disappear paralleled with severe brain atrophy (Ukisu et al., 2005). However, these pathological changes manifest as functional impairment, are consistent and can be detected by sensitive PET measures, which may warrant clinical consideration.

Previous studies have suggested that thalamic involvement is a diagnostic feature of variant CJD (vCJD) (Zeidler et al., 2000), and thalamic involvement has also been occasionally reported in the MM2 thalamic form of sCJD (Hirose et al., 2006; Moda et al., 2012). In addition, one case of VV2 type sCJD also reported changes in the thalamus (Fukushima et al., 2004). These findings suggest that there may be some sleep disturbance and thalamic impairment in sCJD group. However, insomnia was not a common complaint in our sCJD group, and thalamic involvement was not as pronounced in the sCJD group as that in the E200K group. Of note, the MM2-thalamic variant and VV2 variant are rare, comprising 2% and 1% of the patients with sCJD, respectively (Parchi et al., 1999). Although insomnia was observed a common symptom in patients with E200K gCJD in our study, it should be reported with caution due to the small sample size. Previous studies of E200K gCJD have shown significant phenotypic heterogeneity, with observation of unusual symptoms including auditory agnosia, monoparesis, stroke-like presentation, facial nerve palsy, pseudobulbar syndrome, alien hand syndrome, and neurosensorial hypoacusis (Cohen et al., 2016; Necpál et al., 2016; Reñé et al., 2007). The phenotypic heterogeneity may be due to environmental or ethnic factors and need confirmation in a larger cohort.

The clinical spectrum of prion disease may overlap. This study provided clinical-neuroimaging evidence for the phenotypic spectrum of E200K that some features of the E200K phenotype are somewhere in between typical CJD and FFI, which with more predominant insomnia-thalamic impairment. This reminds us of that predominant insomnia-thalamic phenotype might be indicative of specific genotypes including PRNP D178N FFI or E200K gcJD. This clinical variability also attracts the attention of physicians that insomnia should also be

emphasized in E200K gCJD patients, and professional sleep management and treatment should be considered. All these findings help to improve the awareness of physicians to identify the potential CJD patients with E200K mutations and then facilitate early genetic tests, which contributes to the further patient counseling guidance and implementation of management strategies.

Our study had some limitations. First, the sample size was relatively small because of the rarity of CJD which bring bias to the data interpretation. In addition, completion of the hybrid PET/MRI examination was challenging in our patient cohort because of the variable disease condition. Second, the results reported in this study should be considered exploratory which need further investigation. Third, the cross-sectional design weakened drawing of conclusions regarding causality.

5. Conclusion

The clinical and imaging characteristics of patients with gCJD with PRNP E200K mutations were frequently like those observed in fatal familial insomnia, which manifests as a thalamic-insomnia phenotype, indicating that underlying thalamic pathological changes may result from E200K mutations. PET was a sensitive approach to identify functional changes in the thalamus in prion disease.

Funding

This work was supported by grants from the National Natural Science Foundation of China [no.81971011]; Ministry of Science and Technology of China [no. 2019YFC0118600]; and Beijing Municipal Science and Technology Committee [D171100008217005, 7202060].

CRediT authorship contribution statement

Hong Ye: Conceptualization, Methodology, Software, Writing – original draft. **Min Chu:** Conceptualization, Methodology, Software, Writing – original draft. **Zhongyun Chen:** Data curation. **Kexin Xie:** Visualization, Investigation. **Li Liu:** Visualization, Investigation. **Haitian Nan:** . **Yue Cui:** . **Jing Zhang:** Supervision. **Lin Wang:** Supervision. **Junjie Li:** Supervision. **Liyong Wu:** Conceptualization, Methodology, Software, Supervision, Writing – review & editing.

Declaration of Competing Interest

The authors declare that they have no known competing financial interests or personal relationships that could have appeared to influence the work reported in this paper.

Appendix A. Supplementary data

Supplementary data to this article can be found online at https://doi.org/10.1016/j.nicl.2022.103086.

References

Chapman, J., Arlazoroff, A., Goldfarb, L.G., Cervenakova, L., Neufeld, M.Y., Werber, E., Herbert, M., Brown, P., Gajdusek, D.C., Korczyn, A.D., 1996. Fatal insomnia in a case of familial Creutzfeldt-Jakob disease with the codon 200(Lys) mutation. Neurology 46, 758–761.

Chen, C., Dong, X., 2016. Epidemiological characteristics of human prion diseases. Infectious diseases of poverty 5, 47.

Chung, Y.L., Williams, A., Ritchie, D., Williams, S.C., Changani, K.K., Hope, J., Bell, J.D., 1999. Conflicting MRI signals from gliosis and neuronal vacuolation in prion diseases. NeuroReport 10, 3471–3477.

Cohen, O.S., Chapman, J., Korczyn, A.D., Nitsan, Z., Appel, S., Hoffmann, C., Rosenmann, H., Kahana, E., Lee, H., 2015a. Familial Creutzfeldt-Jakob disease with the E200K mutation: longitudinal neuroimaging from asymptomatic to symptomatic CJD. J. Neurol. 262, 604–613.

Cohen, O.S., Chapman, J., Korczyn, A.D., Warman-Alaluf, N., Orlev, Y., Givaty, G., Nitsan, Z., Appel, S., Rosenmann, H., Kahana, E., Shechter-Amir, D., 2015b. Characterization of sleep disorders in patients with E200K familial Creutzfeldt-Jakob disease. J. Neurol. 262, 443–450.

Cohen, O.S., Kimiagar, I., Korczyn, A.D., Nitsan, Z., Appel, S., Hoffmann, C., Rosenmann, H., Kahana, E., Chapman, J., 2016. Unusual presentations in patients with E200K familial Creutzfeldt-Jakob disease. Eur. J. Neurol. 23, 871–877.

Eisenmenger, L., Porter, M.C., Carswell, C.J., Thompson, A., Mead, S., Rudge, P., Collinge, J., Brandner, S., Jäger, H.R., Hyare, H., 2016. Evolution of Diffusion-Weighted Magnetic Resonance Imaging Signal Abnormality in Sporadic Creutzfeldt-Jakob Disease, With Histopathological Correlation. JAMA Neurol. 73, 76–84.

Feketeova, E., Jarcuskova, D., Janakova, A., Vitkova, M., Dragasek, J., Gdovinova, Z., 2019. The insomnia phenotype in genetic Creutzfeldt-Jakob disease based on the E200K mutation. Prion 13, 77–82.

Fukushima, R., Shiga, Y., Nakamura, M., Fujimori, J., Kitamoto, T., Yoshida, Y., 2004. MRI characteristics of sporadic CJD with valine homozygosity at codon 129 of the prion protein gene and PrPSc type 2 in Japan. J. Neurol. Neurosurg. Psychiatry 75, 485–487.

George, P., Newey, C.R., Mente, K.P., Pioro, E.P., 2017. Positron emission tomography imaging in a case of E200K mutation-related spongiform encephalopathy with non-diagnostic magnetic resonance imaging and cerebrospinal fluid testing. SAGE Open Med. Case Rep. 5, 2050313x17700347.

Givaty, G., Maggio, N., Cohen, O.S., Blatt, I., Chapman, J., 2016. Early pathology in sleep studies of patients with familial Creutzfeldt-Jakob disease. J. Sleep Res. 25, 571–575.

Heinemann, U., Krasnianski, A., Meissner, B., Varges, D., Kallenberg, K., Schulz-Schaeffer, W., Steinhoff, B., Grasbon-Frodl, E., Kretzschmar, H., Zerr, I., 2007. Creutzfeldt-Jakob disease in Germany: a prospective 12-year surveillance. Brain 130, 1350–1359.

Hermann, P., Appleby, B., Brandel, J., Caughey, B., Collins, S., Geschwind, M., Green, A., Haïk, S., Kovacs, G., Ladogana, A., Llorens, F., Mead, S., Nishida, N., Pal, S., Parchi, P., Pocchiari, M., Satoh, K., Zanusso, G., Zerr, I., 2021. Biomarkers and diagnostic guidelines for sporadic Creutzfeldt-Jakob disease. Lancet. Neurol. 20, 235–246.

Hirose, K., Iwasaki, Y., Izumi, M., Yoshida, M., Hashizume, Y., Kitamoto, T., Sahashi, K., 2006. MM2-thalamic-type sporadic Creutzfeldt-Jakob disease with widespread neocortical pathology. Acta Neuropathol. 112, 503–511.

Knight, R., Will, R.G., 2004. Prion diseases. J. Neurol. Neurosurg. Psychiatry 75 (Suppl 1), i36–i42.

Konno, S., Murata, M., Toda, T., Yoshii, Y., Nakazora, H., Nomoto, N., Sugimoto, H., Nemoto, H., Wakata, N., Fujioka, T., Kurihara, T., 2008. Familial Creutzfeldt-Jakob Disease with a codon 200 mutation presenting as thalamic syndrome: diagnosis by single photon emission computed tomography using (99m)Tc-ethyl cysteinate dimer. Intern. Med. 47, 65–67.

Kovács, G., Puopolo, M., Ladogana, A., Pocchiari, M., Budka, H., van Duijn, C., Collins, S., Boyd, A., Giulivi, A., Coulthart, M., Delasnerie-Laupretre, N., Brandel, J., Zerr, I., Kretzschmar, H., de Pedro-Cuesta, J., Calero-Lara, M., Glatzel, M., Aguzzi, A., Bishop, M., Knight, R., Belay, G., Will, R., Mitrova, E., 2005. Genetic prion disease: the EUROCJD experience. Hum. Genet. 118, 166–174.

Kovacs, G.G., Seguin, J., Quadrio, I., Höftberger, R., Kapás, I., Streichenberger, N., Biacabe, A.G., Meyronet, D., Sciot, R., Vandenberghe, R., Majtenyi, K., László, L., Ströbel, T., Budka, H., Perret-Liaudet, A., 2011. Genetic Creutzfeldt-Jakob disease associated with the E200K mutation: characterization of a complex proteinopathy. Acta Neuropathol. 121, 39–57.

Manners, D.N., Parchi, P., Tonon, C., Capellari, S., Strammiello, R., Testa, C., Tani, G., Malucelli, E., Spagnolo, C., Cortelli, P., Montagna, P., Lodi, R., Barbiroli, B., 2009. Pathologic correlates of diffusion MRI changes in Creutzfeldt-Jakob disease. Neurology 72, 1425–1431.

Marini, G., Ceccarelli, P., Mancia, M., 2000. Effects of bilateral microinjections of ibotenic acid in the thalamic reticular nucleus on delta oscillations and sleep in freely-moving rats. J. Sleep Res. 9, 359–366.

Moda, F., Suardi, S., Di Fede, G., Indaco, A., Limido, L., Vimercati, C., Ruggerone, M., Campagnani, I., Langeveld, J., Terruzzi, A., Brambilla, A., Zerbi, P., Fociani, P., Bishop, M.T., Will, R.G., Manson, J.C., Giaccone, G., Tagliavini, F., 2012. MM2-thalamic Creutzfeldt-Jakob disease: neuropathological, biochemical and transmission studies identify a distinctive prion strain. Brain Pathol. 22, 662–669.

Necpál, J., Stelzer, M., Koščová, S., Patarák, M., 2016. A Corticobasal Syndrome Variant of Familial Creutzfeldt-Jakob Disease with Stroke-Like Onset. Case Rep. Neurol. Med. 2016, 4167391.

Parchi, P., Giese, A., Capellari, S., Brown, P., Schulz-Schaeffer, W., Windl, O., Zerr, I., Budka, H., Kopp, N., Piccardo, P., Poser, S., Rojiani, A., Streichemberger, N., Julien, J., Vital, C., Ghetti, B., Gambetti, P., Kretzschmar, H., 1999. Classification of sporadic Creutzfeldt-Jakob disease based on molecular and phenotypic analysis of 300 subjects. Ann. Neurol. 46, 224–233.

Qi, C., Zhang, J.T., Zhao, W., Xing, X.W., Yu, S.Y., 2020. Sporadic Creutzfeldt-Jakob Disease: A Retrospective Analysis of 104 Cases. Eur. Neurol. 83, 65–72.

Reñé, R., Campdelacreu, J., Ferrer, I., Escrig, A., Povedano, M., Gascón-Bayarri, J., Moral, E., 2007. Familial Creutzfeldt-Jakob disease with E200K mutation presenting with neurosensorial hypoacusis. J. Neurol. Neurosurg. Psychiatry 78, 103–104.

Saper, C.B., Scammell, T.E., Lu, J., 2005. Hypothalamic regulation of sleep and circadian rhythms. Nature 437, 1257–1263.

Steriade, M., Deschênes, M., Domich, L., Mulle, C., 1985. Abolition of spindle oscillations in thalamic neurons disconnected from nucleus reticularis thalami. J. Neurophysiol. 54, 1473–1497.

Taratuto, A.L., Piccardo, P., Reich, E.G., Chen, S.G., Sevlever, G., Schultz, M., Luzzi, A.A., Rugiero, M., Abecasis, G., Endelman, M., Garcia, A.M., Capellari, S., Xie, Z., Lugaresi, E., Gambetti, P., Dlouhy, S.R., Ghetti, B., 2002. Insomnia associated with thalamic involvement in E200K Creutzfeldt-Jakob disease. Neurology 58, 362–367.

Ukisu, R., Kushihashi, T., Kitanosono, T., Fujisawa, H., Takenaka, H., Ohgiya, Y., Gokan, T., Munechika, H., 2005. Serial diffusion-weighted MRI of Creutzfeldt-Jakob disease. AJR Am. J. Roentgenol. 184, 560–566.
Vitali, P., Maccagnano, E., Caverzasi, E., Henry, R.G., Haman, A., Torres-Chae, C., Johnson, D.Y., Miller, B.L., Geschwind, M.D., 2011. Diffusion-weighted MRI hyperintensity patterns differentiate CJD from other rapid dementias. Neurology 76, 1711–1719.
Zeidler, M., Sellar, R.J., Collie, D.A., Knight, R., Stewart, G., Macleod, M.A., Ironside, J. W., Cousens, S., Colchester, A.C., Hadley, D.M., Will, R.G., 2000. The pulvinar sign on magnetic resonance imaging in variant Creutzfeldt-Jakob disease. Lancet 355, 1412–1418.